How Do Defects in Carbon Nanostructures Regulate the Photoinduced Electron Transfer Processes? The Case of Phenine Nanotubes

Olga A. Stasyuk,*[a] Anton J. Stasyuk,*[a, b] Miquel Solà,*[a] and Alexander A. Voityuk*[a, c]

Photoinduced electron transfer is studied in a series of inclusion complexes of structurally modified phenine nanotubes (**pNT**) with **C$_{70}$** using the TD-DFT method. Analysis of electronic properties of the complexes shows that the electron transfer is infeasible in **pNT_4d⊃C$_{70}$** built on the tetrameric array of [6] cyclo-meta-phenylene ([6]CMP) units. However, replacing one or more [6]CMP units with a coronene moiety enables electron transfer from **pNT** to **C$_{70}$**. The generation of the charge separated states from the lowest locally excited states occurs on a sub-nanosecond time scale. Depending on the number of the [6]CMP units, the charge recombination rate varies from $1.8 \cdot 10^7$ to $3.1 \cdot 10^2$ s^{-1}, i.e., five orders of magnitude.

1. Introduction

Carbon nanotubes (CNTs) are extended cylindrical molecules composed exclusively of hexagonal units of sp^2 hybridized carbon atoms. Since their discovery in 1991,[1] CNTs have drawn enduring attention of researchers due to their unique structural, thermal, electronic, and dynamic properties.[2–4] The combination of these properties makes CNTs one of the most promising elements of nanoelectronics.[5–7] The most advantageous approach to synthesis of structurally uniform CNTs is the bottom-up organic synthesis using carbon nanorings as templates and aliphatic alcohols[8] as the carbon source.[9,10] The use of π-extended nanorings constructed of polyaromatic hydrocarbons as a template can be of considerable advantage. The synthesis of the nanorings on the basis of conjugated polyaromatic hydrocarbons, such as naphthalene, chrysene, pyrene, and even gigantic hexa-peri-hexabenzocoronene (HBC) has already been reported.[11–14]

The introduction of structural entities, such as topological defects, vacancies, and deformations in CNTs greatly increases their diversity and strongly affects their properties. The formation of the modified systems usually takes place during the growth process of CNT or may be caused by external factors.[15] It has been demonstrated that the inclusion of structural defects even in small amounts can dramatically change electronic transport in nanotubes.[16–18] The controlled modification of a nanotube appears to be an extremely tempting approach allowing its properties to be fine-tuned.

Recently, Sun et al.[19] reported CNT-like molecules made up of non-conjugated benzene rings synthesized by replacing the trigonal sp^2-carbon atoms of the CNT with trigonal 1,3,5-trisubstituted benzene (phenine) units. Such nanotubes known as phenine nanotubes (**pNT**) possess six-atom vacancy defects that occur periodically in the cylindrical graphite sheets.

Furthermore, the segments of the carbon nanotubes can serve as hosts for π-conjugated molecules with a convex surface, such as fullerenes.[20] The formation of supramolecular host–guest complexes has been reported for many nanorings as well as **pNTs**.[19] Very recently, we have compared photoinduced electron transfer (PET) properties for 1:1 inclusion complexes of **C$_{70}$** fullerene with cyclic tetramer of hexa-peri-hexabenzocoronene ([**4**]CHBC), which is structurally similar to **pNT**.[21] We have found that the charge transfer states can efficiently be populated in the [**4**]CHBC⊃C$_{70}$ complex, while the vacancy defects in the **pNT**⊃C$_{70}$ dramatically change its electronic character and electron transfer becomes infeasible. The completely different response of [**4**]CHBC⊃C$_{70}$ and **pNT** ⊃C$_{70}$ to photoexcitation prompted us to consider in detail the effect of the structural changes in **pNT** on the PET properties of the host-guest complexes.

Here we report a TD-DFT study of the electronic properties for inclusion complexes of the fullerene **C$_{70}$** and **pNTs** that have different numbers of vacancies. We show that the number of such defects can strongly influence the PET properties of the complexes by activating or deactivating charge separation, and determining the effectiveness of charge recombination processes.

[a] Dr. O. A. Stasyuk, Dr. A. J. Stasyuk, Prof. M. Solà, Prof. A. A. Voityuk
Institut de Química Computacional and Departament de Química, Universitat de Girona, C/ Maria Aurèlia Capmany 69, 17003 Girona, Spain
E-mail: o.a.stasuk@gmail.com
antony.stasuk@gmail.com
miquel.sola@udg.edu
alexander.voityuk@gmail.com

[b] Dr. A. J. Stasyuk
Faculty of Chemistry, University of Warsaw, Pasteura 1, 02-093 Warsaw, Poland

[c] Prof. A. A. Voityuk
Institució Catalana de Recerca i Estudis Avancats (ICREA), 08010 Barcelona, Spain

ChemPhysChem

Articles
doi.org/10.1002/cphc.202100285

Chemistry
Europe
European Chemical
Societies Publishing

2. Results and Discussion

2.1. Ground State Properties

The **pNT** can be considered as a tetrameric array of [6]cyclo-meta-phenylenes ([6]CMP). It contains four six-atom vacancies as compared with **[4]CHBC**. By systematically replacing [6]CMP with HBC units, we obtain five **pNT_xd** structures, where the integer **x** is in the range of 0 to 4 and **d** means the six-atom vacancy defect (see Figure 1). In order to study the influence of the number of vacancy defects on the PET, we consider 1:1 complexes of each **pNT_xd** with the fullerene **C$_{70}$** (Figure 1) in their equilibrium geometries. The ground state (GS) geometries of the modeled complexes were optimized at the BLYP-D3(BJ)/def2-SVP level of theory (see computational methods for details). The stability of wavefunction was tested for each complex. A biradical nature of the systems was tested using broken-symmetry technique. In all cases, the closed-shell singlet state was found to be the lowest.

To estimate the stability of the complexes, the interaction energy (ΔE_{int}) between nanotubes and fullerene were computed. For **pNT_4d⊃C$_{70}$**, **pNT_3d⊃C$_{70}$**, **pNT_2d⊃C$_{70}$**, **pNT_1d⊃C$_{70}$**, and **pNT_0d⊃C$_{70}$** systems, ΔE_{int} is found to be -78.6, -86.4, -77.3, -90.3, and -86.4 kcal/mol, correspondingly. As seen, ΔE_{int} does not regularly depend on **x**. For **pNT_4d⊃C$_{70}$** and **pNT_0d⊃C$_{70}$** complexes, two conformers were found. In each case, one conformer corresponds to a center-symmetric structure, where **C$_{70}$** is in the middle of the **pNT** unit, while **pNTs** maintain their geometry shape as in the free state. The second conformer has an asymmetric structure with the fullerene close to the wall of **pNTs** with notable geometrical distortions but maximizing dispersion interactions. For both complexes, the asymmetric conformer corresponds to the global minimum and its interaction energy is twice as strong as in the symmetric conformer (see Figure S1, SI).

In order to gain an access to the host-guest interaction topology, we performed a series of QTAIM[22,23] calculations. The electron density, its Laplacian, bond critical points (BCPs) and other topological parameters were considered (see Table S1). The analysis revealed two types of host-guest interactions: the π···π interaction between the π-electron systems of the subunits and the CH···π interaction between CH groups of [6]CMP and π-electrons of fullerene. BCPs corresponding to the CH···π interaction were detected in **pNT_4d⊃C$_{70}$** and **pNT_3d⊃C$_{70}$**, while in other complexes only π···π interactions were observed. In all complexes, the π···π interaction is the dominant one (Figure S2, SI). Additionally, we compared the non-covalent interaction (NCI) index.[24] In **pNT_4d⊃C$_{70}$**, the NCI isosurface is represented by two distinct areas in front of two [6]CMP units. Replacing [6]CMP with HBC in **pNT_3d⊃C$_{70}$** slightly increases the NCI isosurface by partially distributing it over the coronene unit. In **pNT_2d⊃C$_{70}$** and **pNT_1d⊃C$_{70}$**, the NCI isosurfaces are located exactly opposite the coronenes. Replacing the [6]CMP unit with a coronene in **pNT_1d⊃C$_{70}$** does not notably change the isosurface. Thus, the NCI and QTAIM tools provide the consistent description of the non-covalent interactions in the complexes. The gradient plots of the reduced density and the NCI isosurfaces are shown in Figures S3 and S4, SI.

As seen from Figure 1, the electronic structure of the host **pNT_4d** differs significantly from the others. In particular, its HOMO is about 1 eV lower in energy than the HOMO in the other tubes but its LUMO is 0.6–0.9 eV higher than the other LUMOs. We note that the orbital energies of **pNT_4d** are similar to the orbital energies of its subunit – 1,3,5-triphenylbenzene with the HOMO and LUMO energies of -7.493 and -0.082 eV. In the host-guest complexes, LUMO is localized on **C$_{70}$**, and its ability to withdraw the electronic density is somewhat lower than that of the isolated fullerene. The changes in LUMO energies are between 0.32 to 0.45 eV, depending on the complex. The energetics of HOMO, which is located on the
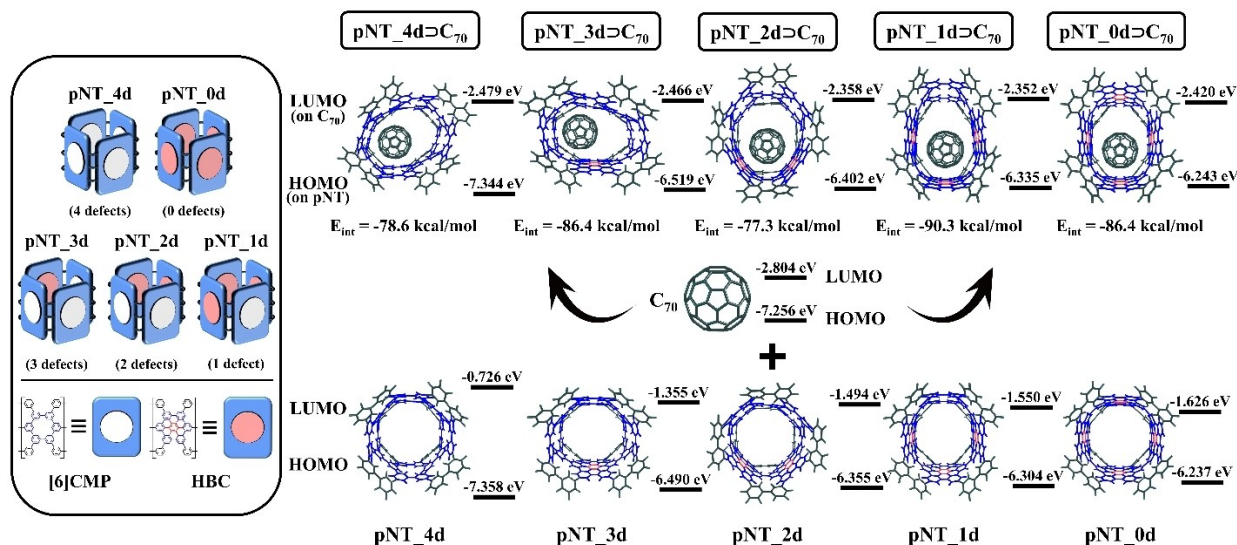

Figure 1. Structures of the studied complexes and their HOMO and LUMO energies. The blue rectangle with the red center denotes hexa-peri-hexabenzocoronene unit, while the rectangle with the white center denotes [6]CMP unit.

pNT_xd unit, remains almost unchanged (it varies by less than 0.05 eV due to the complex formation).

2.2. Singlet Excited States

Simulations of excited states were carried out by TD-DFT method at the CAM-B3LYP-D3(BJ)/def2-SVP//BLYP-D3(BJ)/def2-SVP level of theory. The studied complexes were divided into 2 fragments: host (**pNT_xd**) and guest (**C_{70}**); and the electronic density distribution was analyzed for 50 lowest excited states. Three types of excited states were identified: (1) locally excited (LE) states, where excitation is mostly localized either on **C_{70}** (LE$_1$) or on the host molecule (LE$_2$) with charge separation (CS) smaller than 0.1 e (CS < 0.1 e); (2) charge transfer (CT) states with the electron density transferred between the fragments and significant charge separation is observed (CS > 0.8 e); and (3) mixed states where both LE and CT states contribute substantially (0.1 $e <$ CS < 0.8 e).

In all studied complexes, LE$_1$ states on **C_{70}** are the lowest-lying excited states with similar energy in the range of 2.20 to 2.28 eV. The LE$_2$ states on host are about 1 eV higher in energy. Note that no LE$_2$ state is found within the studied energy range for **pNT_4d$\supset$C$_{70}$** complex. Only one type of CT states, Host$^{+\bullet}$, Guest$^{-\bullet}$, was found among the 50 lowest excited states. As expected, the corresponding transitions GS→CT have weak oscillator strengths (f < 0.001). The energy of the CT states depends heavily on the number of the vacancy defects in the host molecule and ranges from 3.49 eV for **pNT_4d$\supset$C$_{70}$** to 2.44 eV for **pNT_0d$\supset$C$_{70}$** (see Table 1). The decrease in energy is due to a higher electron-donor ability of the host unit when passing from **pNT_4d** to **pNT_0d**. This in turn leads to a dramatic change of the energy gap between LE$_1$ and CT states. The gap decreases from 1.21 eV in **pNT_4d$\supset$C$_{70}$** to 0.21 eV in **pNT_0d$\supset$C$_{70}$** complex. The CT states Host$^{\bullet}$ Guest$^{+\bullet}$ with opposite direction of electron transfer have a significantly

higher energy and are beyond the 50 lowest excited states. In addition, we analyzed selected excited states with the natural transition orbital (NTO) method (Figure 2). The NTOs representing the LE$_1$, LE$_2$, and CT states for all of the complexes examined are shown in Figures S5–S9.

The electronic properties of semiconducting carbon nanotubes, such as HOMO and LUMO energies, and HOMO − LUMO gap, have been demonstrated to converge rapidly within a small number of carbon atoms.[25,26] To estimate the effect of the length of a phenine nanotube on its electronic properties, we considered a series of extended nanotubes based on **pNT_0d** model. The smallest nanotube has 264 carbon atoms, whereas the biggest system is almost twice as large and consists of 504 carbon atoms (Figure 3).

We showed earlier that the HOMO energy of the considered **pNT_xd** nanotubes does not change upon the formation of complexes with C_{70} fullerene. Thus, the effect of the size of **pNT_xd** on the electron donating properties can be well described by the HOMO energy of the nanotube. As seen from Figure 3, the HOMO energy of a nanotube changes only within 0.1 eV with an increase in its size (Table S2, Figure S10). Thus, for the phenine nanotubes, no significant effect of length on their electron-donating properties is expected.

2.3. Environmental Effects

A COSMO-like model using the monopole approximation was applied to estimate the influence of polar environment on electronic excitations.[27–30] Dichloromethane (DCM) was taken as the solvent. The ground state solvation energies of **pNT_4d$\supset$C$_{70}$**, **pNT_3d$\supset$C$_{70}$**, **pNT_2d$\supset$C$_{70}$**, **pNT_1d$\supset$C$_{70}$**, and **pNT_0d$\supset$C$_{70}$** systems are found to be −0.22, −0.18, −0.23, −0.22, and −0.21 eV, respectively. The similarity of the solvation energies can be explained by similar values of the dipole moment in the GS state (it varies between 0.19 and 0.37D, see Table S3).

Table 1. Singlet excitation energies (*Ex*, eV), main singly excited configuration (HOMO(H)-LUMO(L)) and its weight (W), oscillator strength (f), and extent of charge separation (CT, e) or exciton localization (X) in the host-guest systems in the gas phase.

	pNT_4d$\supset$C$_{70}$	pNT_3d$\supset$C$_{70}$	pNT_2d$\supset$C$_{70}$	pNT_1d$\supset$C$_{70}$	pNT_0d$\supset$C$_{70}$
			Supramolecular host-guest systems		
			LE$_1$ (Guest C$_{70}$)		
Ex	2.276	2.264	2.232	2.242	2.219
Transition (W)	H–L+2 (0.45)	H-2–L+1 (0.23)	H-1–L+2 (0.27)	H-1–L+1 (0.23)	H-1–L (0.42)
f	0.001	0.004	<0.001	0.001	0.004
X	0.933	0.905	0.864	0.875	0.865
			LE$_2$ (Host)		
Ex	n/f[*]	3.228	3.209	3.178	3.186
Transition (W)		H–L+6 (0.28)	H–L+3 (0.53)	H-2–L+3 (0.25)	H-3–L+3 (0.17)
f		0.079	0.236	0.224	0.363
X		0.705	0.751	0.753	0.844
			CT (Host→Fullerene C$_{70}$)		
Ex	3.490	2.746	2.530	2.534	2.435
Transition (W)	H-8–L (0.12)	H–L+1 (0.35)	H–L (0.73)	H–L+1 (0.33)	H–L (0.57)
f	<0.001	<0.001	<0.001	<0.001	<0.001
CT	0.895	0.815	0.972	0.925	0.907

[*] n/f – states of interest are not found within considered number of excited states. C_{70} lowest singlet excited state energy $Ex = 2.32$ eV.
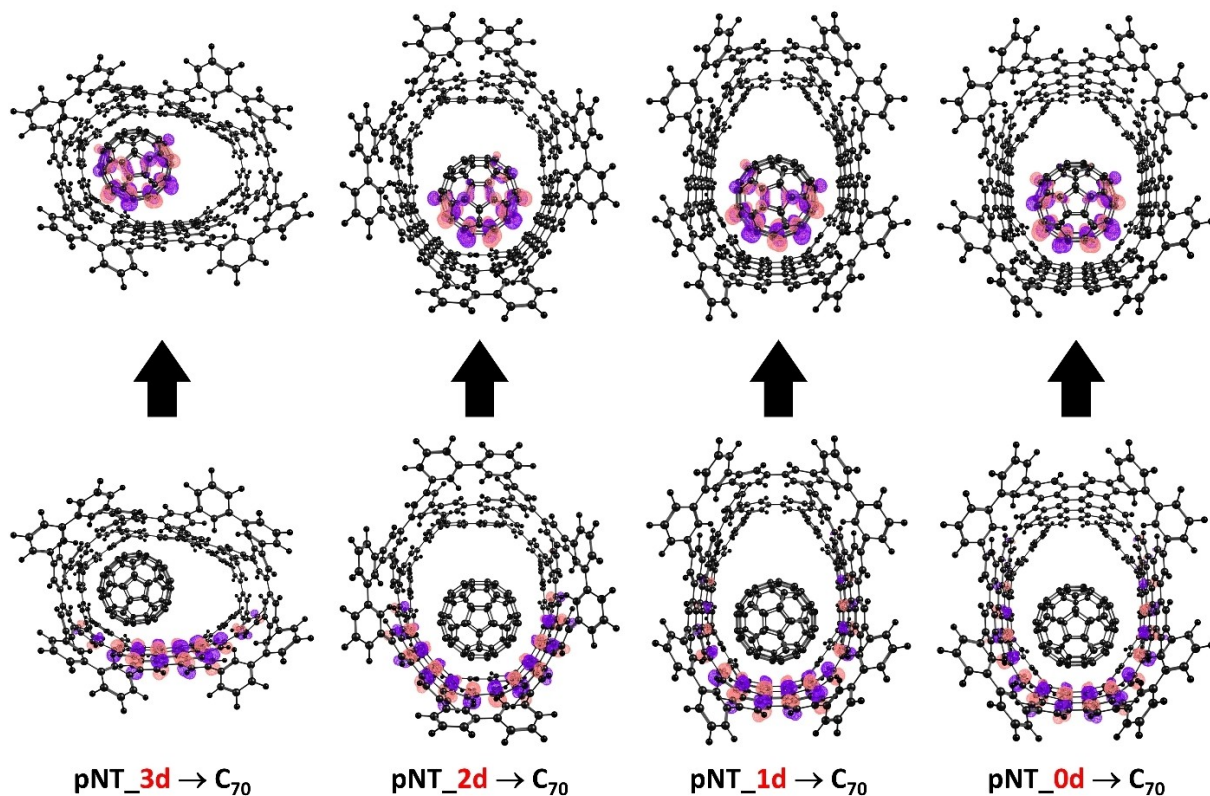
Figure 2. Natural transition orbitals representing CT state for **pNT_3d⊃C$_{70}$, pNT_2d⊃C$_{70}$, pNT_1d⊃C$_{70}$** and **pNT_0d⊃C$_{70}$** complexes.
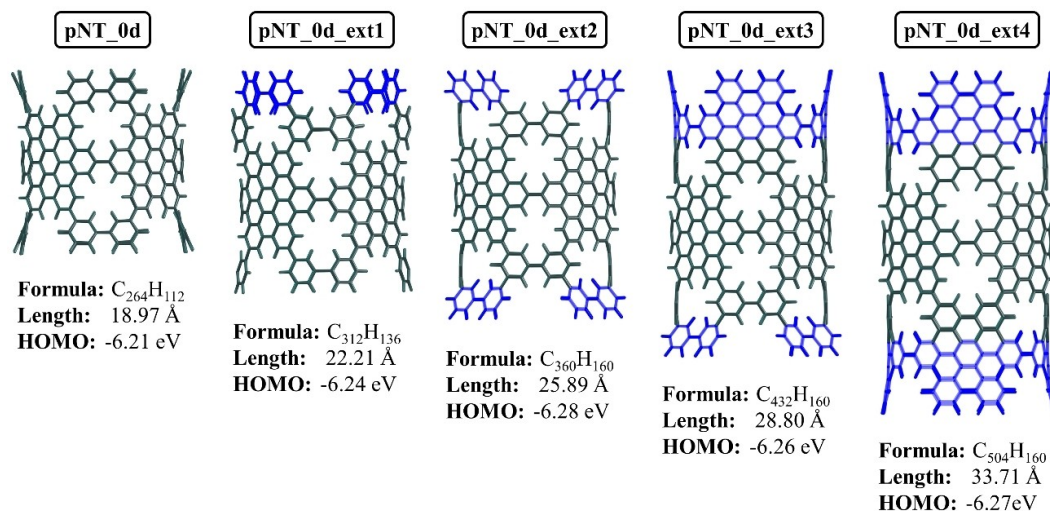

Figure 3. Structures of extended phenine nanotubes based on **pNT_0d**, their lengths and HOMO energies.

Keeping in mind that the inclusion **C$_{70}$** unit is a strong electron acceptor, we calculated GS charge separation values. The population analysis performed within several of the most common schemes (Table S4, SI) did not reveal any significant charge transfer between the host and guest molecules. As expected, the solvation energies of the LE states are very similar to those of the ground state, while clear differences are found for the CT states. The ability of both fragments to effectively delocalize the charge, however, gives a reason for rather small changes in the dipole moments between GS and CT states and for the relatively small solvation energies of the CT states. In the series from **pNT_4d⊃C$_{70}$** to **pNT_0d⊃C$_{70}$**, an almost twofold decrease (from −0.76 to −0.45 eV) in the solvation energy of CT states was observed (see Table S3, SI). This can be rationalized by a different charge delocalization over the fragments in the CT state. The inverse participation ratio (IPR) that counts the

ChemPhysChem

Articles
doi.org/10.1002/cphc.202100285

**Chemistry
Europe**
European Chemical
Societies Publishing

number of atoms over which the transferred charge has been delocalized is a useful tool for quantifying the charge delocalization on each fragment. The IPR values for **pNT_4d, pNT_3d, pNT_2d, pNT_1d**, and **pNT_0d** fragments are 14.3, 39.5, 54.4, 56.2, and 61.0, respectively. In turn, IPR value for the **C$_{70}$** unit in the complexes is similar and varies from 31.4 to 38.8 (see Table S5, SI). Thus, the observed difference in the solvation energies of CT states correlates with the IPR index for the host fragment, i.e., the more the charge is localized, the larger is the stabilization by the solvent. Figure 4 displays the energies of GS, LE, and CT states for studied complexes in DCM. As seen, the solvent stabilization of the CT state in **pNT_4d⊃C$_{70}$** is insufficient to reorder the CT and the LE states by passing from the gas phase to DCM. However, in the systems with at least one coronene unit, the energies of the CT and LE$_1$ states become very similar and the gap between them varies from 0.07 to −0.02 eV, thus allowing an efficient population of the CT state by electron transfer between the fragments.

2.4. Electron Transfer Rates

GS→CT transitions in the complexes are characterized by a very weak oscillator strength (f < 0.001, Table 1), and therefore the CT states cannot be populated effectively by light absorption. However, they can be generated by the decay of the lowest LE state. The semi-classical method proposed by Ulstrup and Jortner[31,32] was used to compute the rates of charge separation (CS) and charge recombination (CR). Within this approach, the rate of electron transfer is controlled by four parameters: electronic coupling $|V_{ij}|$ of the initial and the final states, solvation reorganization energy λ_s, reaction Gibbs energy ΔG^0, and effective Huang-Rhys factor S_{eff} as a function of the internal reorganization energy λ_i (for details see SI). The CS and CR rates were computed using the effective frequency of 1600 cm^{-1}, which corresponds to the stretching of C=C bonds. Note that the calculated charge separation rates for nanoring-fullerene inclusion complexes do not change significantly by varying the effective frequency from 1400 to 1800 cm^{-1}.[21,33] Table 2 shows
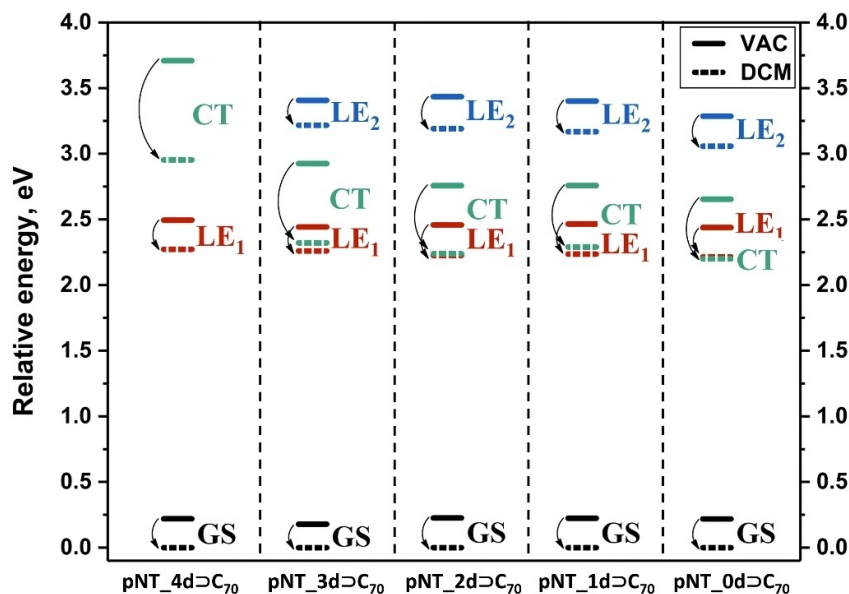

Figure 4. Relative energies (in eV) of GS, LE, and CT states in the **pNT_4d⊃C$_{70}$**, **pNT_3d⊃C$_{70}$**, **pNT_2d⊃C$_{70}$**, **pNT_1d⊃C$_{70}$**, and **pNT_0d⊃C$_{70}$** complexes computed in vacuum (VAC) and dichloromethane (DCM).

Table 2. Gibbs energies ΔG^0 (in eV), electronic coupling $|V_{ij}|$ (in eV), solvent (λ_s) and internal (λ_i) reorganization energies (in eV), Huang-Rhys factor (S_{eff}) and rate constants k (in s^{-1}) for CS (highlighted in green) and CR processes in **pNT_4d⊃C$_{70}$**, **pNT_3d⊃C$_{70}$**, **pNT_2d⊃C$_{70}$**, **pNT_1d⊃C$_{70}$**, and **pNT_0d⊃C$_{70}$** complexes in DCM.

| Complex | Transition | $\Delta G^{0[a]}$, eV | $|V_{ij}|$, eV | Reorg. Energy, eV | | $S_{eff}^{[b]}$ | k, s^{-1} |
				λ_i	λ_s		
pNT_4d⊃C$_{70}$	LE$_1$→CT	0.680	4.40·10^{-3}	0.165	0.271	0.832	[4.93·10^{-3}]
pNT_3d⊃C$_{70}$	LE$_1$→CT	0.062	2.68·10^{-3}	0.258	0.210	1.301	8.55·10^9
	CT→GS	−2.322	2.23·10^{-2}	0.271	0.210	1.366	1.81·10^7
pNT_2d⊃C$_{70}$	LE$_1$→CT	0.012	1.22·10^{-3}	0.205	0.139	1.033	1.36·10^{10}
	CT→GS	−2.238	1.37·10^{-3}	0.236	0.139	1.190	3.95·10^4
pNT_1d⊃C$_{70}$	LE$_1$→CT	0.054	1.31·10^{-3}	0.162	0.117	0.817	7.41·10^9
	CT→GS	−2.290	1.61·10^{-3}	0.189	0.117	0.953	1.14·10^3
pNT_0d⊃C$_{70}$	LE$_1$→CT	−0.021	1.89·10^{-3}	0.148	0.114	0.746	8.50·10^{10}
	CT→GS	−2.208	1.41·10^{-3}	0.150	0.114	0.756	3.08·10^2

[a] Gibbs energy difference between denoted states in corresponding solvent. [b] An effective Huang-Rhys factor $S_{eff} = \lambda_i / \hbar\omega_{eff}$, where $\hbar\omega_{eff}$ set to 1600 cm^{-1}.

ChemPhysChem

Articles
doi.org/10.1002/cphc.202100285

Chemistry
Europe
European Chemical
Societies Publishing

the computed rates for CS and CR reactions in the considered systems.

As seen in Table 2, the charge separation in **pNT_4d⊃C₇₀** has a positive Gibbs energy which makes PET unlikely. For other systems, the charge separation reaction occurs in the normal Marcus regime ($|\Delta G_0| < \lambda$) on a picosecond time scale, while the charge recombination takes place in a deeply inverted Marcus region ($|\Delta G_0| \gg \lambda$). Important to note that both CS and CR rates depend on the number of the vacancy defects in **pNTs**. Although the CS rate varies in the range of $8.6 \cdot 10^9$ to $8.5 \cdot 10^{10}$ s^{-1}, the CR rate decreases dramatically when the number of the vacancies is reduced (Figure 5).

In **pNT_3d⊃C₇₀** with only one coronene unit, population of the CT state occurs on a sub-nanosecond time scale ($k_{CS} = 8.5 \cdot 10^9$ s^{-1}). Also, the CR reaction is fast ($k_{CR} = 1.8 \cdot 10^7$ s^{-1}) and can act as an effective deactivation channel of the CT state, thereby preventing long distance separation of the ion pairs. The subsequent decrease in the number of vacancies ([6]CMP subunits) accelerates the CS reaction slightly ($k_{CS} = 1.4 \cdot 10^{10}$ s^{-1}) but slows the CR significantly ($k_{CR} = 3.9 \cdot 10^4$ s^{-1}). In **pNT_0d⊃C₇₀**, the CS process is fast, while the CR reaction is very slow (Table 2, Figure 5). This is the most favorite situation for efficient photoinduced separation of electrons and holes that can be applied in photovoltaic devices.

3. Conclusions

The TD-DFT study of five inclusion complexes of phenine nanotubes **pNT_xd** (**x** changes from 0 to 4) with fullerene **C₇₀** has revealed that photoinduced charge transfer is not possible in **pNT_4d⊃C₇₀** complex built on the tetrameric array of [6] CMP. However, the replacement of at least one of the [6]CMP subunits by the coronene moiety enables the charge separation

process. The CT states with the electron transfer from **pNT_xd** to **C₇₀** in **pNT_3d⊃C₇₀**, **pNT_2d⊃C₇₀**, **pNT_1d⊃C₇₀**, and **pNT_0d⊃C₇₀** can be generated by the decay of the lowest LE states. This process occurs on a sub-nanosecond time scale. The number of vacancy defects dramatically affects the rate of the charge recombination. The CR rate decreases by more than four orders of magnitude when passing from the **pNT_3d⊃C₇₀** to **pNT_0d⊃C₇₀**. Thus, the vacancy defects in phenine nanotubes dramatically change the electronic properties of their inclusion fullerene complexes. Varying the number of vacancies in **pNTs** is a powerful tool for tuning their photophysical properties.

Computational methods

Quantum Chemical Calculations

Geometry optimization of the complexes was performed employing the DFT BLYP[34,35] exchange−correlation functional with Ahlrichs' def2-SVP basis set,[36,37] and using the resolution of identity approximation (RI, alternatively termed density fitting)[38,39] implemented in the ORCA 4.2.1 program.[40,41] The host-guest interaction energy was computed using BLYP functional coupled with triple-ξ def2-TZVP basis set.[42] Vertical excitation energies were calculated using TDA formalism[43] with the range-separated functional from Handy and coworkers' CAM−B3LYP[44] and Ahlrichs' def2-SVP basis set, using Gaussian 16 (rev. A03).[45] The empirical dispersion D3 correction with Becke–Johnson damping was employed.[46,47] The population analysis performed within Mulliken,[48,49] Lowdin,[50] Hirshfeld,[51] and CM5[52] schemes were carried out using code implemented in Gaussian 16. Topological analysis of the electron density distribution was conducted within the "Quantum Theory of Atoms in Molecules" (QTAIM) approach[22,23] using AIMALL suite of programs.[53] The NCI method[24,54] was employed through the analysis of the reduced density gradient (RDG) at the CAM-B3LYP/ def2-SVP level using Multiwfn program.[55]
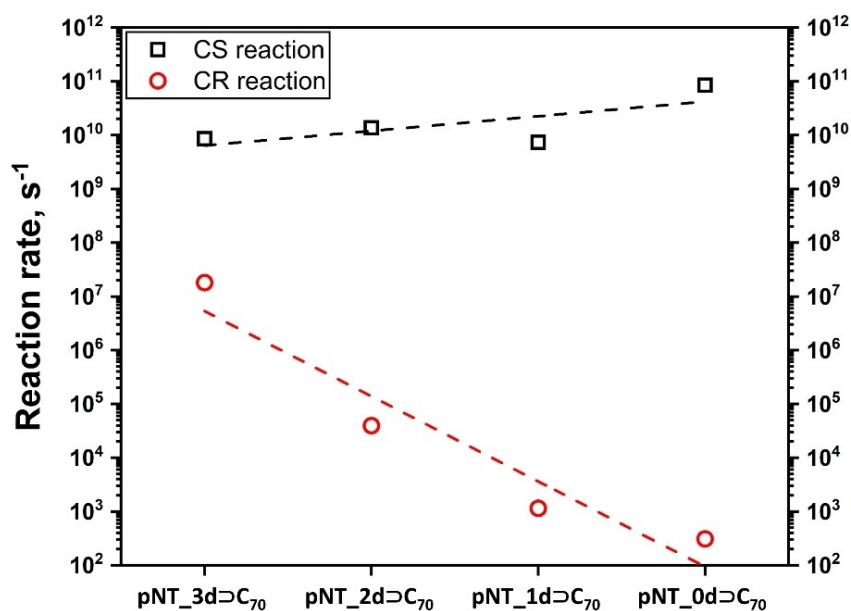

Figure 5. Charge separation and charge recombination rates as a function of the number of vacancy defects in the pNTs.

The excited states have been analyzed in terms of the natural transition orbitals (NTO) concept introduced by Luzanov *et al.*[56] and implemented within modern many-body codes by Head-Gordon *et al.*[57] To visualize molecular structures, NCI isosurfaces, and natural transition orbitals, the Chemcraft 1.8. program was used.[58]

Analysis of Excited States

The quantitative analysis of exciton delocalization and charge transfer in the donor-acceptor complexes is carried out in terms of transition density.[59–61] The analysis is convenient to perform in the Löwdin orthogonalized basis. The matrix $^\lambda\mathbf{C}$ of orthogonalized MO coefficients is obtained from the coefficients $\mathbf{C}$ in the original basis $^\lambda\mathbf{C} = \mathbf{S}^{1/2}\,\mathbf{C}$, where $\mathbf{S}$ is the atomic orbital overlap matrix. The transition density matrix T^{0i} for an excited state Φ^* constructed as a superposition of singly excited configurations (where an occupied MO ψ_i is replaced a virtual MO ψ_a) is computed as

$$T^{0i}_{\alpha\beta} = \sum_{ia} A^{\lambda}_{i\to a} C^{\lambda}_{\alpha i} C_{\beta a} \tag{1}$$

Where $A_{i\to a}$ is the expansion coefficient.

A key quantity $\Omega(D,A)$ is determined by

$$\Omega(D,A) = \sum_{\alpha\in D,\ \beta\in A} \left(T^{0i}_{\alpha\beta}\right)^2 \tag{2}$$

The weights of local excitations on D and A are $\Omega(D,D)$ and $\Omega(A,A)$. The weight of electron transfer configurations D→A and A→D is represented by $\Omega(D,A)$ and $\Omega(A,D)$, respectively. The index Δq, which describes charge separation and charge transfer between D and A, is

$$\Delta q(CS) = \sum \Omega(D,A) - \Omega(A,D) \tag{3}$$

$$\Delta q(CT) = \sum \Omega(D,A) + \Omega(A,D) \tag{4}$$

Solvent Effects

The equilibrium solvation energy E_S^{eq} of a molecule (in the ground or excited state) in the medium with the dielectric constant ε was estimated using a COSMO-like polarizable continuum model[29,30] in monopole approximation:

$$E_S^{eq}(Q,\varepsilon) = -\frac{1}{2}f(\varepsilon)Q^+DQ \tag{5}$$

where the $f(\varepsilon)$ is the dielectric scaling factor, $f(\varepsilon) = 1 - 1/\varepsilon$, $\mathbf{Q}$ is the vector of n atomic charges in the molecular system, and $\mathbf{D}$ is the $n\times n$ symmetric matrix determined by the shape of the boundary surface between solute and solvent. $\mathbf{D} = \mathbf{B}^+\mathbf{A}^{-1}\mathbf{B}$, where the $m\times m$ matrix $\mathbf{A}$ describes electrostatic interaction between m surface charges and the $m\times n$ $\mathbf{B}$ matrix describes the interaction of the surface charges with n atomic charges of the solute.[62–64] The GEPOL93 scheme[65] was used to construct the molecular boundary surface.

The charge on atom X in the excited state Φ_i, q_X^i, was calculated as:

$$q_X^i = q_X^0 + \Delta_X^i, \quad \Delta_X^i = \sum_{Y\neq X}\sum_{\alpha\in X,\ \beta\in Y}(T^{0i}_{\alpha\beta}T^{0i}_{\alpha\beta} - T^{0i}_{\beta\alpha}T^{0i}_{\beta\alpha}), \tag{6}$$

where q_X^0 is the atomic charge on A in the ground state and Δ_X^i is its change due to the redistribution of the electron density between the atoms X and Y which is caused by the excitation $\psi_0 \to \psi_i$.

The non-equilibrium solvation energy for excited state ψ_i can be estimated as:[66]

$$E_S^{neq}(Q^0,\Delta,\varepsilon,n^2) = f(\varepsilon)\Delta^+DQ^0 - \frac{1}{2}f(n^2)\Delta^+D\Delta, \tag{7}$$

In Eq. (7), n^2 (the refraction index squared) is the optical dielectric constant of the medium and the vector Δ describes the change of atomic charges in the molecule by excitation in terms of atomic charges, see Eq. (6). By definition, the external (solvent) reorganization energy is the difference of the non-equilibrium (Eq. 7) and equilibrium solvation (Eq. 5) energies of the excited state.

Electron Transfer Rates

The rate of the nonadiabatic ET, k_{ET}, can be expressed in terms of the electronic coupling squared, V^2, and the Franck-Condon Weighted Density of states (FCWD):

$$k_{ET} = \frac{2\pi}{\hbar}V^2\ (FCWD) \tag{8}$$

that accounts for the overlap of vibrational states of donor and acceptor and can be approximately estimated using the classical Marcus equation:[67]

$$(FCWD) = (4\pi\lambda kT)^{-1/2}\exp\left[-(\Delta G^0 + \lambda)^2/4\lambda kT\right] \tag{9}$$

where λ is the reorganization energy and ΔG^0 is the standard Gibbs energy change of the process. The fragment charge difference (FCD)[68,69] method was employed to calculate the electronic couplings in this work.

The Marcus expression is derived for the high-temperature condition, $\hbar\omega_l \ll kT$, for all vibrational modes l. The semi-classical description of electron transfer (ET)[31,32] includes the effect of the quantum vibrational modes in an effective way, the solvent (low frequency) modes are treated classically, while a single high-frequency intramolecular mode ω_i, $\hbar\omega_i \gg kT$, is described quantum mechanically. Because ET occurs normally from the lowest vibrational level of the initial state, the rate k can be expressed as a sum over all channels connecting the initial state with the vibrational quantum number n=0 to manifold vibrational levels of the final state,

$$k = \sum_{n=0}^{\infty} k_{0\to n},\ \text{where}\ k_{0\to n} = \frac{2\pi}{\hbar}V^2_{0\to n}\frac{1}{\sqrt{4\pi\lambda_s kT}}\exp$$
$$\left[-\frac{(\Delta G + \nu\hbar\omega_i + \lambda_s)^2}{4\lambda_s kT}\right] \tag{10}$$

with

$$V_{0 \to n}^2 = V^2 \frac{S^n}{n!} \exp(-S) \qquad (11)$$

An effective value of the Huang-Rhys factor S is estimated from the internal reorganization energy λ_i,

$$S = \lambda_i / \hbar \omega_i$$

As seen, an additional parameter (as compared to the Marcus equation) enters the semi-classical expression - the frequency ω_i of a vibrational mode that effectively describes the nuclear intramolecular relaxation following the ET. Typically, in organic systems (including fullerene and nanotube derivatives) the main contribution to the internal reorganization energy is due to stretching of C=C bonds (the corresponding frequencies are found to be in the range 1400–1800 cm^{-1}). Thus, the effective frequency was set to 1600 cm^{-1}.

Charge Delocalization Index

The degree of electron delocalization in the state of interest is quantified by the inverse participation ratio (IPR):

$$IPR = \Delta q^F \left(\sum_i^n \frac{1}{(\Delta q_i^F)^2} \right) \qquad (12)$$

where Δq^F – indicates charge difference on the fragment in charge separated state compare to the ground state, while $(\Delta q_i^F)^2$ – corresponds to square of particular atom charge difference for denoted fragment in CS state compare to GS.

Author contributions

O. A. S. Investigation, Formal analysis, Writing – original draft, Writing – review & editing. A. J. S. Investigation, Formal analysis, Writing – original draft, Writing – review & editing. M. S. Supervision, Writing – review & editing, Funding acquisition. A. A. V. Supervision, Writing – review & editing

Acknowledgements

Conflict of Interest

The authors declare no conflict of interest.

[1] S. Iijima, *Nature* **1991**, *354*, 56–58.
[2] R. H. Baughman, A. A. Zakhidov, W. A. De Heer, *Science* **2002**, *297*, 787–792.
[3] D. Tasis, N. Tagmatarchis, A. Bianco, M. Prato, *Chem. Rev.* **2006**, *106*, 1105–1136.
[4] V. Harik, in *Mechanics of Carbon Nanotubes* (Ed.: V. Harik), Academic Press 2018, pp. 1–24.
[5] W. B. Choi, E. Bae, D. Kang, S. Chae, B. H. Cheong, J. H. Ko, E. Lee, W. Park, *Nanotechnology* **2004**, *15*, S512–S516.
[6] Y. Che, H. Chen, H. Gui, J. Liu, B. Liu, C. Zhou, *Semicond. Sci. Technol.* **2014**, *29*, 073001.
[7] Q. Cao, S. Han, in *Nanomaterials, Polymers and Devices: Materials Functionalization and Device Fabrication* (Ed.: E. S. W. Kong), Wiley-VCH, Weinheim 2015, pp. 501–521.
[8] H. Omachi, T. Nakayama, E. Takahashi, Y. Segawa, K. Itami, *Nat. Chem.* **2013**, *5*, 572–576.
[9] H. Omachi, Y. Segawa, K. Itami, *Acc. Chem. Res.* **2012**, *45*, 1378–1389.
[10] E. H. Fort, P. M. Donovan, L. T. Scott, *J. Am. Chem. Soc.* **2009**, *131*, 16006–16007.
[11] S. E. Lewis, *Chem. Soc. Rev.* **2015**, *44*, 2221–2304.
[12] D. Lu, G. Zhuang, H. Wu, S. Wang, S. Yang, P. Du, *Angew. Chem. Int. Ed.* **2017**, *56*, 158–162; *Angew. Chem.* **2017**, *129*, 164–168.
[13] E. J. Leonhardt, R. Jasti, *Nat. Rev. Chem.* **2019**, *3*, 672–686.
[14] D. Wu, W. Cheng, X. Ban, J. Xia, *Asian J. Org. Chem.* **2018**, *7*, 2161–2181.
[15] J. C. Charlier, *Acc. Chem. Res.* **2002**, *35*, 1063–1069.
[16] P. G. Collins, A. Zettl, H. Bando, A. Thess, R. E. Smalley, *Science* **1997**, *278*, 100.
[17] J. A. Robinson, E. S. Snow, Ş. C. Baˇdescu, T. L. Reinecke, F. K. Perkins, *Nano Lett.* **2006**, *6*, 1747–1751.
[18] L. Chico, L. X. Benedict, S. G. Louie, M. L. Cohen, *Phys. Rev. B* **1996**, *54*, 2600–2606.
[19] Z. Sun, K. Ikemoto, T. M. Fukunaga, T. Koretsune, R. Arita, S. Sato, H. Isobe, *Science* **2019**, *363*, 151–155.
[20] D. Lu, Q. Huang, S. Wang, J. Wang, P. Huang, P. Du, *Front. Chem.* **2019**, *7*, 668.
[21] A. J. Stasyuk, O. A. Stasyuk, M. Solà, A. A. Voityuk, *Chem. Commun.* **2020**, *56*, 12624–12627.
[22] R. F. W. Bader, *Chem. Rev.* **1991**, *91*, 893–928.
[23] R. F. W. Bader, *Atoms in Molecules: A Quantum Theory; International Series of Monographs on Chemistry 22*; Oxford University Press: Oxford, U. K., **1990**.
[24] E. R. Johnson, S. Keinan, P. Mori-Sánchez, J. Contreras-García, A. J. Cohen, W. Yang, *J. Am. Chem. Soc.* **2010**, *132*, 6498–6506.
[25] M. Baldoni, A. Sgamellotti, F. Mercuri, *Org. Lett.* **2007**, *9*, 4267–4270.
[26] O. A. Stasyuk, A. J. Stasyuk, A. A. Voityuk, M. Solà, *J. Org. Chem.* **2020**, *85*, 11721–11731.
[27] A. J. Stasyuk, O. A. Stasyuk, S. Filippone, N. Martin, M. Solà, A. A. Voityuk, *Chem. Eur. J.* **2018**, *24*, 13020–13025.
[28] A. J. Stasyuk, O. A. Stasyuk, M. Solà, A. A. Voityuk, *Phys. Chem. Chem. Phys.* **2019**, *21*, 25098–25107.
[29] A. A. Voityuk, S. F. Vyboishchikov, *Phys. Chem. Chem. Phys.* **2019**, *21*, 18706–18713.
[30] A. A. Voityuk, S. F. Vyboishchikov, *Phys. Chem. Chem. Phys.* **2020**, *22*, 14591–14598.
[31] J. Ulstrup, J. Jortner, *J. Chem. Phys.* **1975**, *63*, 4358–4368.
[32] J. Jortner, *J. Chem. Phys.* **1976**, *64*, 4860–4867.
[33] A. J. Stasyuk, O. A. Stasyuk, M. Solà, A. A. Voityuk, *J. Phys. Chem. B* **2020**, *124*, 9095–9102.
[34] A. D. Becke, *Phys. Rev. A* **1988**, *38*, 3098–3100.
[35] C. Lee, W. Yang, R. G. Parr, *Phys. Rev. B* **1988**, *37*, 785–789.
[36] F. Weigend, R. Ahlrichs, *Phys. Chem. Chem. Phys.* **2005**, *7*, 3297–3305.
[37] F. Weigend, *Phys. Chem. Chem. Phys.* **2006**, *8*, 1057–1065.
[38] K. Eichkorn, O. Treutler, H. Öhm, M. Häser, R. Ahlrichs, *Chem. Phys. Lett.* **1995**, *240*, 283–290.
[39] K. Eichkorn, F. Weigend, O. Treutler, R. Ahlrichs, *Theor. Chem. Acc.* **1997**, *97*, 119–124.
[40] F. Neese, *WIREs Comput. Mol. Sci.* **2012**, *2*, 73–78.
[41] F. Neese, *WIREs Comput. Mol. Sci.* **2017**, *8*, e1327.
[42] K. Eichkorn, F. Weigend, O. Treutler, R. Ahlrichs, *Theor. Chem. Acc.* **1997**, *97*, 119.

[43] S. Hirata, M. Head-Gordon, *Chem. Phys. Lett.* **1999**, *314*, 291–299.

[44] T. Yanai, D. P. Tew, N. C. Handy, *Chem. Phys. Lett.* **2004**, *393*, 51–57.

[45] *Gaussian 16*, Revision A.03, M. J. Frisch, G. W. Trucks, H. B. Schlegel, G. E. Scuseria, M. A. Robb, J. R. Cheeseman, G. Scalmani, V. Barone, G. A. Petersson, H. Nakatsuji, X. Li, M. Caricato, A. V. Marenich, J. Bloino, B. G. Janesko, R. Gomperts, B. Mennucci, H. P. Hratchian, J. V. Ortiz, A. F. Izmaylov, J. L. Sonnenberg, D. Williams-Young, F. Ding, F. Lipparini, F. Egidi, J. Goings, B. Peng, A. Petrone, T. Henderson, D. Ranasinghe, V. G. Zakrzewski, J. Gao, N. Rega, G. Zheng, W. Liang, M. Hada, M. Ehara, K. Toyota, R. Fukuda, J. Hasegawa, M. Ishida, T. Nakajima, Y. Honda, O. Kitao, H. Nakai, T. Vreven, K. Throssell, J. A. Montgomery, Jr., J. E. Peralta, F. Ogliaro, M. J. Bearpark, J. J. Heyd, E. N. Brothers, K. N. Kudin, V. N. Staroverov, T. A. Keith, R. Kobayashi, J. Normand, K. Raghavachari, A. P. Rendell, J. C. Burant, S. S. Iyengar, J. Tomasi, M. Cossi, J. M. Millam, M. Klene, C. Adamo, R. Cammi, J. W. Ochterski, R. L. Martin, K. Morokuma, O. Farkas, J. B. Foresman, D. J. Fox, Gaussian, Inc., Wallingford CT, 2016.

[46] S. Grimme, J. Antony, S. Ehrlich, H. Krieg, *J. Chem. Phys.* **2010**, *132*, 154104.

[47] S. Grimme, S. Ehrlich, L. Goerigk, *J. Comput. Chem.* **2011**, *32*, 1456–1465.

[48] R. S. Mulliken, *J. Chem. Phys.* **1955**, *23*, 1833–1840.

[49] R. S. Mulliken, *J. Chem. Phys.* **1955**, *23*, 1841–1846.

[50] P. O. Löwdin, *J. Chem. Phys.* **1950**, *18*, 365–375.

[51] F. L. Hirshfeld, *Theor. Chim. Acta* **1977**, *44*, 129–138.

[52] A. V. Marenich, S. V. Jerome, C. J. Cramer, D. G. Truhlar, *J. Chem. Theory Comput.* **2012**, *8*, 527–541.

[53] Keith, T. A. *AIMAll*, version 14.06.21; TK Gristmill Software: Overland Park, KS, 2014.

[54] J. Contreras-García, E. R. Johnson, S. Keinan, R. Chaudret, J. Piquemal, D. Beratan, W. Yang, *J. Chem. Theory Comput.* **2011**, *7*, 625–632.

[55] T. Lu, F. Chen, *J. Comput. Chem.* **2012**, *33*, 580–592.

[56] A. V. Luzanov, A. A. Sukhorukov, V. E. Umanskii, *Theor. Exp. Chem.* **1976**, *10*, 354–361.

[57] M. Head-Gordon, A. M. Grana, D. Maurice, C. A. White, *J. Phys. Chem.* **1995**, *99*, 14261–14270.

[58] G. A. Zhurko, *Chemcraft* 1.80 (build 523b) - graphical program for visualization of quantum chemistry computations. (https://chemcraft-prog.com).

[59] F. Plasser, H. Lischka, *J. Chem. Theory Comput.* **2012**, *8*, 2777–2789.

[60] F. Plasser, S. A. Bäppler, M. Wormit, A. Dreuw, *J. Chem. Phys.* **2014**, *141*, 024107.

[61] A. V. Luzanov, O. A. Zhikol, *Int. J. Quantum Chem.* **2010**, *110*, 902–924.

[62] B. Mennucci, *WIREs Comput. Mol. Sci.* **2012**, *2*, 386–404.

[63] A. Klamt, G. Schüürmann, *J. Chem. Soc. Perkin Trans.* **1993**, *2*, 799–805.

[64] J. Tomasi, B. Mennucci, R. Cammi, *Chem. Rev.* **2005**, *105*, 2999–3093.

[65] J. L. Pascual-Ahuir, E. Silla, I. Tuñón, *J. Comp. Chem.* **1994**, *15*, 1127–1138.

[66] A. Klamt, *J. Phys. Chem.* **1996**, *100*, 3349–3353.

[67] R. A. Marcus, N. Sutin, *Biochim. Biophys. Acta, Rev. Bioenerg.* **1985**, *811*, 265–322.

[68] A. A. Voityuk, N. Rösch, *J. Chem. Phys.* **2002**, *117*, 5607–5616.

[69] A. A. Voityuk, *Phys. Chem. Chem. Phys.* **2012**, *14*, 13789–13793.